

# Design of an optimized MoS<sub>2</sub>-based highly sensitive near-infrared surface plasmon resonance imaging biosensor

YI XU,<sup>1</sup> LIN WU,<sup>2</sup> AND LAY KEE ANG<sup>1,\*</sup>

<sup>1</sup>*SUTD-MIT International Design Center, Singapore University of Technology and Design, Singapore 487372*

<sup>2</sup>*Institute of High Performance Computing, Agency for Science, Technology, and Research (A\*STAR), 1 Fusionopolis Way, #16-16 Connexis, Singapore 138632*

\*[ricky\\_ang@sutd.edu.sg](mailto:ricky_ang@sutd.edu.sg)

**Abstract:** A surface plasmon resonance imaging biosensor based on MoS<sub>2</sub> deposited on Aluminium substrate is designed for high imaging sensitivity and detection accuracy. The proposed biosensor exhibits better performance than graphene-based biosensor in the near-infrared regime. A high imaging sensitivity of more than 970 RIU<sup>-1</sup> is obtained at the wavelength of 1540 nm. The effect of aluminium thickness, number of MoS<sub>2</sub> layers and the refractive index of sensing layer are investigated to obtain an optimized design for high sensor performance. In addition, the sensor performance comparison of MoS<sub>2</sub> and other two-dimensional transition metal dichalcogenide materials based biosensor in the near-infrared regime are also presented. The designed MoS<sub>2</sub> mediated surface plasmon resonance imaging biosensor could provide potential applications in surface plasmon resonance imaging detection of multiple biomolecular interactions simultaneously.

© 2021 Optical Society of America under the terms of the [OSA Open Access Publishing Agreement](#)

**OCIS codes:** (240.6680) Surface plasmons; (280.4788) Optical sensing and sensors; (280.1415) Biological sensing and sensors.

## References and links

1. J. Homola, S. S. Yee, and G. Gauglitz, "Surface plasmon resonance sensors: review," *Sens. Actuators B Chem.* **54**(1-2), 3–15 (1999).
2. J. Homola, "Surface plasmon resonance sensors for detection of chemical and biological species," *Chem. Rev.* **108**(2), 462–493 (2008).
3. X. Fan, I. M. White, S. I. Shopova, H. Zhu, J. D. Suter, and Y. Sun, "Sensitive optical biosensors for unlabeled targets: A review," *Anal. Chim. Acta* **620**(1-2), 8–26 (2008).
4. E. Wijaya, C. Lenaerts, S. Maricot, J. Hastanin, S. Habraken, J.-P. Vilcot, R. Boukherroub, and S. Szunerits, "Surface plasmon resonance-based biosensors: From the development of different spr structures to novel surface functionalization strategies," *Curr. Op. Sol. St. M.* **15**(5), 208–224 (2011).
5. E. Kretschmann and H. Raether, "Notizen: radiative decay of non radiative surface plasmons excited by light," *Z. Naturforsch. A* **23**(12), 2135–2136 (1968).
6. A. W. Wark, H. J. Lee, and R. M. Corn, "Long-range surface plasmon resonance imaging for bioaffinity sensors," *Anal. Chem.* **77**(13), 3904–3907 (2005).
7. H. J. Lee, D. Nedelkov, and R. M. Corn, "Surface plasmon resonance imaging measurements of antibody arrays for the multiplexed detection of low molecular weight protein biomarkers," *Anal. Chem.* **78**(18), 6504–6510 (2006).
8. Y. Zeng, R. Hu, L. Wang, D. Gu, J. He, S.-Y. Wu, H.-P. Ho, X. Li, J. Qu, B. Z. Gao, Y. Shao, "Recent advances in surface plasmon resonance imaging: detection speed, sensitivity, and portability," *Nanophotonics* **6**(5), 1017–1030 (2017).
9. S. H. Choi and K. M. Byun, "Investigation on an application of silver substrates for sensitive surface plasmon resonance imaging detection," *J. Opt. Soc. Am. A* **27**(10), 2229–2236 (2010).
10. C. L. Wong and M. Olivo, "Surface plasmon resonance imaging sensors: a review," *Plasmonics* **9**(4), 809–824 (2014).
11. M. W. Knight, N. S. King, L. Liu, H. O. Everitt, P. Nordlander, and N. J. Halas, "Aluminum for plasmonics," *ACS Nano* **8**(1), 834–840 (2013).
12. N. S. King, L. Liu, X. Yang, B. Cerjan, H. O. Everitt, P. Nordlander, and N. J. Halas, "Fano resonant aluminum nanoclusters for plasmonic colorimetric sensing," *ACS Nano* **9**(11), 10628–10636 (2015).
13. W. Li, K. Ren, and J. Zhou, "Aluminum-based localized surface plasmon resonance for biosensing," *TrAC Trends Anal. Chem.* **80**, 486–494 (2016).

14. P. K. Maharana, T. Srivastava, and R. Jha, "Ultrasensitive plasmonic imaging sensor based on graphene and silicon," *IEEE Photon. Technol. Lett.* **25**(2), 122–125 (2013).
15. P. K. Maharana, T. Srivastava, and R. Jha, "On the performance of highly sensitive and accurate graphene-on-aluminum and silicon-based spr biosensor for visible and near infrared," *Plasmonics* **9**(5), 1113–1120 (2014).
16. S. H. Choi, Y. L. Kim, and K. M. Byun, "Graphene-on-silver substrates for sensitive surface plasmon resonance imaging biosensors," *Opt. Express* **19**(2), 458–466 (2011).
17. L. Wu, H. Chu, W. Koh, and E. Li, "Highly sensitive graphene biosensors based on surface plasmon resonance," *Opt. Express* **18**(14), 14395–14400 (2010).
18. A. C. Ferrari, F. Bonaccorso, V. Fal'Ko, K. S. Novoselov, S. Roche, P. Bøggild, S. Borini, F. H. Koppens, V. Palermo, N. Pugno, J. A. Garrido, R. Sordan, A. Bianco, L. Ballerini, M. Prato, E. Lidorikis, J. Kivioja, C. Marinelli, T. Ryhänen, A. Morpurgo, J. N. Coleman, V. Nicolosi, L. Colombo, A. Fert, M. Garcia-Hernandez, A. Bachtold, G. F. Schneider, F. Guinea, C. Dekker, M. Barbone, Z. Sun, C. Galiotis, A. N. Grigorenko, G. Konstantatos, A. Kis, M. Katsnelson, L. Vandersypen, A. Loiseau, V. Morandi, D. Neumaier, E. Treossi, V. Pellegrini, M. Polini, A. Tredicucci, G. M. Williams, B. H. Hong, J. H. Ahn, J. M. Kim, H. Zirath, B. J. van Wees, H. van der Zant, L. Occhipinti, A. Di Matteo, I. A. Kinloch, T. Seyller, E. Quesnel, X. Feng, K. Teo, N. Rupesinghe, P. Hakonen, S. R. T. Neil, Q. Tannock, T. Löfwander, and J. Kinaret, "Science and technology roadmap for graphene, related two-dimensional crystals, and hybrid systems," *Nanoscale* **7**(11), 4598–4810 (2015).
19. F. K. Perkins, A. L. Friedman, E. Cobas, P. Campbell, G. Jernigan, and B. T. Jonker, "Chemical vapor sensing with monolayer mos<sub>2</sub>," *Nano Lett.* **13**(2), 668–673 (2013).
20. S. Zeng, S. Hu, J. Xia, T. Anderson, X.-Q. Dinh, X.-M. Meng, P. Coquet, and K.-T. Yong, "Graphene–mos<sub>2</sub> hybrid nanostructures enhanced surface plasmon resonance biosensors," *Sens. Actuators B Chem.* **207**, 801–810 (2015).
21. A. K. Mishra, S. K. Mishra, and R. K. Verma, "Graphene and beyond graphene mos<sub>2</sub>: a new window in surface-plasmon-resonance-based fiber optic sensing," *J. Phys. Chem. C* **120**(5), 2893–2900 (2016).
22. C. Rao, K. Gopalakrishnan, and U. Maitra, "Comparative study of potential applications of graphene, mos<sub>2</sub>, and other two-dimensional materials in energy devices, sensors, and related areas," *ACS Appl. Mater. Interfaces* **7**(15), 7809–7832 (2015).
23. Q. Ouyang, S. Zeng, L. Jiang, J. Qu, X.-Q. Dinh, J. Qian, S. He, P. Coquet, and K.-T. Yong, "Two-dimensional transition metal dichalcogenide enhanced phase-sensitive plasmonic biosensors: Theoretical insight," *J. Phys. Chem. C* **121**(11), 6282–6289 (2017).
24. Q. Ouyang, S. Zeng, L. Jiang, L. Hong, G. Xu, X.-Q. Dinh, J. Qian, S. He, J. Qu, P. Coquet, K.-T. Yong, "Sensitivity enhancement of transition metal dichalcogenides/silicon nanostructure-based surface plasmon resonance biosensor," *Sci. Rep.* **6**, 28190 (2016).
25. K. Kalantar-zadeh and J. Z. Ou, "Biosensors based on two-dimensional mos<sub>2</sub>," *ACS Sens.* **1**(1), 5–16 (2015).
26. D. Sarkar, W. Liu, X. Xie, A. C. Anselmo, S. Mitragotri, and K. Banerjee, "Mos<sub>2</sub> field-effect transistor for next-generation label-free biosensors," *ACS Nano* **8**(4), 3992–4003 (2014).
27. J. Lee, P. Dak, Y. Lee, H. Park, W. Choi, M. A. Alam, and S. Kim, "Two-dimensional layered mos<sub>2</sub> biosensors enable highly sensitive detection of biomolecules," *Sci. Rep.* **4**, 7352 (2014).
28. O. Lopez-Sanchez, D. Lembke, M. Kayci, A. Radenovic, and A. Kis, "Ultrasensitive photodetectors based on monolayer mos<sub>2</sub>," *Nat. Nanotechnol.* **8**(7), 497–501 (2013).
29. K. Roy, M. Padmanabhan, S. Goswami, T. P. Sai, G. Ramalingam, S. Raghavan, and A. Ghosh, "Graphene-mos<sub>2</sub> hybrid structures for multifunctional photoresponsive memory devices," *Nat. Nanotechnol.* **8**(11), 826–830 (2013).
30. K. F. Mak, C. Lee, J. Hone, J. Shan, and T. F. Heinz, "Atomically thin mos<sub>2</sub>: a new direct-gap semiconductor," *Phys. Rev. Lett.* **105**, 136805 (2010).
31. D. Lembke, S. Bertolazzi, and A. Kis, "Single-layer mos<sub>2</sub> electronics," *Acc. Chem. Res.* **48**(1), 100–110 (2015).
32. Q. H. Wang, K. Kalantar-Zadeh, A. Kis, J. N. Coleman, and M. S. Strano, "Electronics and optoelectronics of two-dimensional transition metal dichalcogenides," *Nat. Nanotechnol.* **7**(11), 699–712 (2012).
33. A. B. Farimani, K. Min, and N. R. Aluru, "DNA base detection using a single-layer mos<sub>2</sub>," *ACS Nano* **8**(8), 7914–7922 (2014).
34. P. K. Maharana and R. Jha, "Chalcogenide prism and graphene multilayer based surface plasmon resonance affinity biosensor for high performance," *Sens. Actuators B Chem.* **169**, 161–166 (2012).
35. M. Yamamoto, "Surface plasmon resonance (spr) theory: tutorial," *Review of Polarography* **48**, 209–237 (2002).
36. J. Weber, V. Calado, and M. Van de Sanden, "Optical constants of graphene measured by spectroscopic ellipsometry," *Appl. Phys. Lett.* **97**(9), 091904 (2010).
37. S. Yang, C. Jiang, and S.-H. Wei, "Gas sensing in 2D materials," *Appl. Phys. Rev.* **4**(2), 021304 (2017).
38. G. Yang, C. Zhu, D. Du, J. Zhu, and Y. Lin, "Graphene-like two-dimensional layered nanomaterials: applications in biosensors and nanomedicine," *Nanoscale* **7**(34), 14217–14231 (2015).

---

## 1. Introduction

Surface plasmon resonance (SPR), in which surface plasmon waves (SPWs) are excited at the metal-dielectric interface, has been widely employed in the sensing applications over the last few decades [1–4]. Many optical structures have been proposed to excite SPWs [1, 2], like

prism-coupling, waveguide-coupling and grating-coupling. A typical SPW excitation structure is the Kretschmann configuration [5], where a thin metal film is coated over the base of a prism. The SPWs are excited by a p-polarized light when the propagation constant of the incident light along the metal-dielectric interface matches the propagation constant of SPW [1]. The excitation of SPWs depends on the refractive index (RI) of dielectric medium that in contact with the metal thin film. Therefore, SPR can be used to detect the variation of ambient RI. One of the widely used SPR sensing techniques is the angle interrogation scheme, which is a sensitive and robust detection method for SPR sensors. In this approach, a p-polarized monochromatic light is employed to excite SPWs at the metal-dielectric interface, and the reflectance is monitored as a function of the incident angle. However, one limitation of this scheme is its inability to measure diverse sets of samples at a time. SPR imaging sensors [6–10], measure numerous samples in a parallel manner, have been proposed and demonstrated to overcome this limitation. Noted for a SPR imaging sensor, the spatial variations in reflectivity are measured at a fixed incident angle (i.e., no moving parts) due to the ambient RI changes.

Noble metals, like gold and silver, are usually employed to excite SPWs in SPR sensors. However, gold-based SPR sensor shows a broader SPR curve which degrades the detection accuracy. In contrast, aluminium (Al) is a promising material for plasmonics application [11–15] not only because its narrow SPR curve, tunable plasmon resonant from visible to ultraviolet regime, but also for low cost. However, Al is prone to oxidation which will decrease the sensor performances. Recently, two-dimensional (2D) nanomaterials, like graphene, have been proposed to inhibit the oxidation of Al thin film in SPR sensors [14, 15]. Although coating Al thin film with graphene layers will decrease the sensor sensitivity, the protected SPR sensor can still obtain an exceptionally high sensitivity due to the atomic thickness of the 2D nonmaterial.

In addition to the graphene-based SPR sensor [14–18], 2D transition metal dichalcogenides (TMDCs) such as Molybdenum disulfide ( $\text{MoS}_2$ ) have also been widely employed in sensing applications [19–27]. Compared with graphene, monolayer  $\text{MoS}_2$  has a higher optical absorption efficiency ( $\sim 5\%$ ) [28], which provides promising applications in various optoelectronic nanodevices, such as photodetectors with a high responsivity of  $5 \times 10^8 \text{ AW}^{-1}$  [29]. The nonzero tunable band gap of  $\text{MoS}_2$  [30] makes it an attractive candidate for future nanoelectronic devices as well as biosensors [31, 32]. For example, the nonzero bandgap of  $\text{MoS}_2$  can be utilized to fabricate an ultrasensitive field-effect transistor biosensor based on  $\text{MoS}_2$ , while the zero bandgap in graphene limits the sensitivity of graphene-based field-effect transistor biosensor [26]. In addition, the hydrophobic nature of  $\text{MoS}_2$  allows it to be used in biosensors as a recognition layer which exhibits high affinity to biomolecules absorption [27, 33]. All these exciting properties make  $\text{MoS}_2$  a highly potential candidate for biosensing applications. Taking the advantages of SPR imaging sensor, Al and  $\text{MoS}_2$ , a highly sensitive and accurate SPR imaging biosensor based on  $\text{MoS}_2$  deposited on Al thin film has been designed in this paper. The  $\text{MoS}_2$  layer in our designed configuration serves two purposes, as the protective layer of Al thin film and as the recognition layer to capture the biomolecules. We first compared the sensor performance of our design to the graphene-based SPR imaging sensor in the visible and near-infrared regime, which shows that  $\text{MoS}_2$ -based sensor has a better performance in the near-infrared region. By focusing in the near-infrared regime, we have studied various designed parameters in details in order to obtain an optimized performance including the effects of multiple layers of  $\text{MoS}_2$ , thickness of the Al film, and RI of the sensing layer. In addition, the performances of other 2D TMDCs based biosensors have also compared at the end.

## 2. Theoretical Model

The Kretschmann configuration is employed to design our proposed biosensor structure, as shown in Fig. 1. In the proposed design,  $\text{MoS}_2$  coated Al thin film is attached to a chalcogenide (2S2G) glass prism, which is a promising candidate for the design of SPR sensor due to its broad

operating window (from visible to near-infrared regime) and high RI. A p-polarized light with a fixed wavelength is incident at one side of the prism with a fixed incident angle, while the reflected light is collected on the other side.

The wavelength-dependent RI of the 2S2G prism is given by [34]:

$$n_{2S2G} = 2.24047 + \frac{2.693 \times 10^{-2}}{\lambda^2} + \frac{9.08 \times 10^{-3}}{\lambda^4}, \quad (1)$$

where the wavelength  $\lambda$  is given in  $\mu\text{m}$ . The RI of Al is given by

$$n_{\text{Al}} = \left( 1 - \frac{\lambda^2 \lambda_c}{\lambda_p^2 (\lambda_c + i\lambda)} \right)^{1/2}, \quad (2)$$

according to the Drude-Lorentz model [15]. Here,  $\lambda_p$  ( $=1.0657 \times 10^{-7}$  m) and  $\lambda_c$  ( $=2.4511 \times 10^{-5}$  m) is the plasma wavelength and collision wavelength of Al, respectively. The thickness of monolayer MoS<sub>2</sub> is 0.65 nm, and its RI in visible and near-infrared region is shown in Table 1 [23]. The RI of the sensing layer is initially set to  $n_s = 1.330$ .

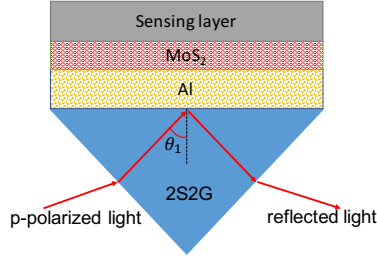


Fig. 1. Schematic of MoS<sub>2</sub>-based SPR imaging sensor.

Table 1. RI of Monolayer MoS<sub>2</sub> in the Near-Infrared Region [23]

wavelength	RI
$\lambda=633$ nm	$5.0805 + i1.1732$
$\lambda=785$ nm	$4.6348 + i0.1163$
$\lambda=904$ nm	$4.7261 + i0.1346$
$\lambda=1150$ nm	$4.4317 + i0.0721$
$\lambda=1540$ nm	$4.2374 + i0.0325$

To obtain the reflectance of the sensor configuration, a generalized N-layer model [35] was employed, and the reflectance  $R$  for the p-polarized incident light is given by

$$R = \frac{\left| (M_{11} + M_{12}q_N)q_1 - (M_{21} + M_{22}q_N) \right|^2}{\left| (M_{11} + M_{12}q_N)q_1 + (M_{21} + M_{22}q_N) \right|^2}, \quad (3)$$

with

$$M = \begin{bmatrix} M_{11} & M_{12} \\ M_{21} & M_{22} \end{bmatrix} = \prod_{k=2}^{N-1} M_k, \quad (4)$$

and

$$M_k = \begin{bmatrix} \cos \beta_k & -i(\sin \beta_k)/q_k \\ -iq_k \sin \beta_k & \cos \beta_k \end{bmatrix}. \quad (5)$$

We denote

$$\beta_k = \frac{2\pi d_k}{\lambda} (n_k^2 - n_1^2 \sin^2 \theta_1), \quad (6)$$

and

$$q_k = \frac{(n_k^2 - n_1^2 \sin^2 \theta_1)^{1/2}}{n_k^2}, \quad (7)$$

where  $n_k$  and  $d_k$  are respectively the RI and thickness of the  $k$ th layer with  $k = 2$  to  $N - 1$ . The first layer ( $k = 1$ ) is the 2S2G prism, and the last layer ( $k = N$ ) is the sensing layer.  $\theta_1$  is the incident angle at the prism-Al interface, and  $\lambda$  is the wavelength of the p-polarized incident light.

A variation of the sensing layer RI ( $n_s$ ) will cause a change in the reflectance  $R$ , and the imaging sensitivity of the SPR sensor is defined as

$$S = \frac{dR}{dn_s}, \quad (8)$$

where the reflectance  $R$  is given in Eq. (3). Besides the imaging sensitivity, another important parameter for the sensor performance is the full width at half maximum (FWHM) of the reflectance curve, which describes the detection accuracy of the sensor. To achieve an excellent performance imaging sensor, we note that the sensor should exhibit high imaging sensitivity and low FWHM (i.e., high detection accuracy).

### 3. Results and discussion

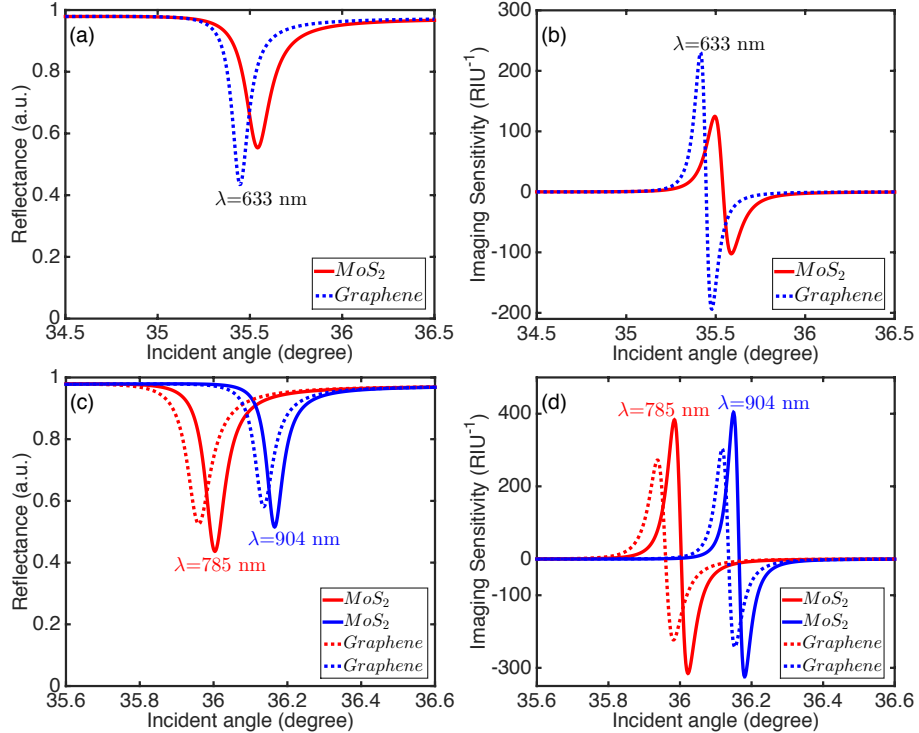


Fig. 2. Reflectance (a)(c) and imaging sensitivity (b)(d) for monolayer MoS<sub>2</sub> and graphene-based sensor at  $\lambda = 633$  nm, 785 nm and 904 nm. The Al thickness is 50 nm.

The reflectance and imaging sensitivity for two sensors: a monolayer MoS<sub>2</sub>-based sensor and graphene-based sensor, both deposited on a 50 nm thick Al film are shown in Fig. 2 for both visible ( $\lambda = 633$  nm) and near-infrared ( $\lambda = 785$  nm and 904 nm) wavelengths. The RI of graphene in the visible and near-infrared region is taken from Ref. [36]. In the visible region ( $\lambda = 633$  nm), graphene-based sensor shows a narrow SPR curve in comparison with that of MoS<sub>2</sub>-based sensor ( $0.1082^\circ$  vs.  $0.1591^\circ$ ), as shown in Fig. 2(a). For the imaging sensitivity, it is found that the sensitivity exhibits a positive peak as well as a negative peak (see Fig. 2(b) and (d)). We only considered the positive peak imaging sensitivity since its magnitude is higher than that of negative peak (see Fig. 2(b) and (d)). In the following, the imaging sensitivity means the positive peak imaging sensitivity. The imaging sensitivity of graphene-based sensor ( $230.4 \text{ RIU}^{-1}$ ) is higher than the sensitivity for MoS<sub>2</sub>-based imaging sensor ( $124.8 \text{ RIU}^{-1}$ ) at  $\lambda = 633$  nm. However, at the near-infrared region ( $\lambda = 785$  nm and 904 nm), the imaging sensitivity of MoS<sub>2</sub>-based sensor is higher than that of graphene-based sensor (see Fig. 2(d) and Table 2). The FWHM of MoS<sub>2</sub>-based sensor in the near-infrared region is smaller than that of graphene-based sensor (see Table 2). Thus the findings of high imaging sensitivity and low FWHM have indicated that MoS<sub>2</sub> based sensor has better performance than graphene-based sensor in the near-infrared region. The trends also indicates its better performance may be extended to even longer wavelengths, and thus we will focus on three longer wavelengths (785 nm, 1150 nm and 1540 nm) in the optical near-infrared regime in the subsequent studies.

Table 2. Comparison of sensor performances for monolayer MoS<sub>2</sub>- and graphene-based sensor in the visible and near-Infrared Region.

wavelength	Imaging Sensitivity ( $\text{RIU}^{-1}$ )		FWHM (degree)	
	MoS <sub>2</sub> -based	graphene-based	MoS <sub>2</sub> -based	graphene-based
$\lambda = 633$ nm	124.8	230.4	0.1591	0.1082
$\lambda = 785$ nm	383.4	272.7	0.0657	0.0772
$\lambda = 904$ nm	403.9	303.6	0.0538	0.0613

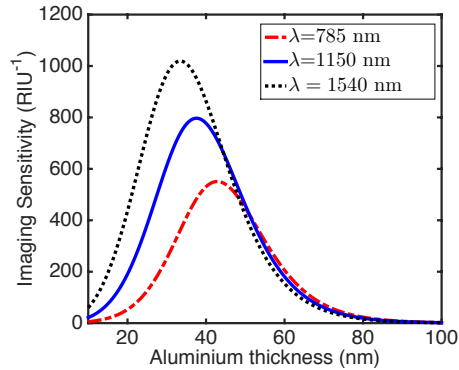


Fig. 3. Imaging sensitivity as a function of the Al thickness without MoS<sub>2</sub> coated.

Before investigating the sensor performance of MoS<sub>2</sub>-based biosensor at longer wavelength, we first optimize the Al thickness since the thickness of plasmonics supporting material is an important parameter for the SPR sensor performance. The imaging sensitivity as a function of the Al thickness (without coated MoS<sub>2</sub>) at wavelengths  $\lambda = 785$  nm, 1150 nm and 1540 nm is shown in Fig. 3. It can be seen from Fig. 3 that the optimized Al thickness decreases with the increasing wavelength. Here, we consider the optimized Al thickness is 38 nm, at which at least

90% of the maximum imaging sensitivity's value can be obtained for all three wavelengths.

The effect of multiple MoS<sub>2</sub> layers on the reflectance and sensor performance at three different wavelengths is shown in Fig. 4. It is found that the resonance curves become shallower and broader (larger FWHM, see Fig. 4(d)) with the number of MoS<sub>2</sub> layers increases, which is a result of the increased surface plasmon damping. For example, with monolayer MoS<sub>2</sub> coated sensor, the FWHM is 0.105° at  $\lambda = 785$  nm, while FWHM is 0.0532° at  $\lambda = 1150$  nm and 0.0343° at  $\lambda = 1540$  nm. When the Al thin film is coated with 20 layers MoS<sub>2</sub>, the FWHM becomes quite large at  $\lambda = 785$  nm (1.249°), while the FWHM at longer wavelength is still small (0.1791° at  $\lambda = 1150$  nm and 0.0755° at  $\lambda = 1540$  nm). In addition, the resonance angle increases with the number of MoS<sub>2</sub> layers. For the imaging sensitivity, it decreases with the increasing number of MoS<sub>2</sub> layers (see Fig. 4(d)) due to the increased loss within the MoS<sub>2</sub> layers. As mentioned before, Al is susceptible to oxidation which decreases the sensor performances, whereas MoS<sub>2</sub> layers deposited on Al thin film can be utilized to inhibit the oxidation of Al. Although coating with MoS<sub>2</sub> decreases the imaging sensitivity, the designed biosensors with monolayer or bilayer MoS<sub>2</sub> can still provide exceptional sensitivities. For monolayer MoS<sub>2</sub>-based sensor, the imaging sensitivity is 442 RIU<sup>-1</sup> at  $\lambda = 785$  nm, 745.8 RIU<sup>-1</sup> at  $\lambda = 1150$  nm and 895.6 RIU<sup>-1</sup> at  $\lambda = 1540$  nm. It is noted that the proposed biosensor provides a relative high sensitivity of 397.8 RIU<sup>-1</sup> at  $\lambda = 1540$  nm with 20 layers MoS<sub>2</sub>, while it is only 36.96 RIU<sup>-1</sup> at  $\lambda = 785$  nm. Higher sensitivity and smaller FWHM are obtained at higher wavelength, which is consistent with the results shown in Fig. 2.

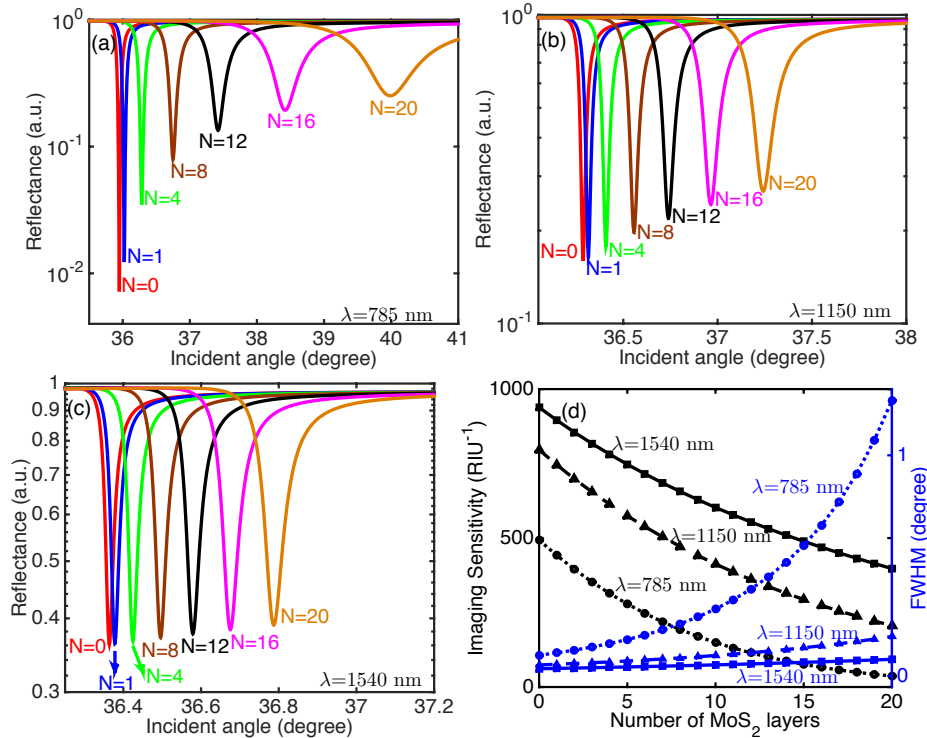


Fig. 4. Reflectance as a function of incident angle for multiple MoS<sub>2</sub>-based SPR imaging sensor at wavelength (a)  $\lambda = 785$  nm, (b)  $\lambda = 1150$  nm and (c)  $\lambda = 1540$  nm. (d) Imaging sensitivity and FWHM for SPR imaging sensor with multiple MoS<sub>2</sub> layers at different wavelengths. The Al thickness is 38 nm.

To optimize the design of MoS<sub>2</sub>-on-Al SPR imaging sensor, Fig. 5 shows the imaging sensitivity

as a function of the number of MoS<sub>2</sub> layers and Al thickness at three different wavelengths: 785 nm, 1150 nm and 1540 nm. For monolayer MoS<sub>2</sub>-based sensor, highest imaging sensitivity of  $\sim 484 \text{ RIU}^{-1}$  is obtained with Al thickness around 42.5 nm at  $\lambda = 785 \text{ nm}$ ,  $\sim 747 \text{ RIU}^{-1}$  with Al thickness  $\sim 37.5 \text{ nm}$  for  $\lambda = 1150 \text{ nm}$ , and  $\sim 974 \text{ RIU}^{-1}$  with Al thickness  $\sim 33.5 \text{ nm}$  at wavelength  $\lambda = 1540 \text{ nm}$ . This indicates that the proposed sensor not only protects the Al from oxidation, but also provides ultrahigh imaging sensitivities. It can be seen from Fig. 5 that the designed sensor shows significantly high imaging sensitivity for few MoS<sub>2</sub> layers with 35-50 nm Al thickness at wavelength  $\lambda = 785 \text{ nm}$ , 30-45 nm Al thickness at  $\lambda = 1150 \text{ nm}$ , and 25-45 nm Al thickness at  $\lambda = 1540 \text{ nm}$ . It is noted that the proposed sensor with 15 layers MoS<sub>2</sub> at  $\lambda = 1150 \text{ nm}$  can still exhibits sensitivity of more than  $300 \text{ RIU}^{-1}$  with Al thickness around 35 nm. Even for Al film coated with 30 MoS<sub>2</sub> layers, the proposed sensor can provide an imaging sensitivity of  $\sim 300 \text{ RIU}^{-1}$  (more than  $290 \text{ RIU}^{-1}$ ) at wavelength  $\lambda = 1540 \text{ nm}$  with Al thickness around 30 nm.

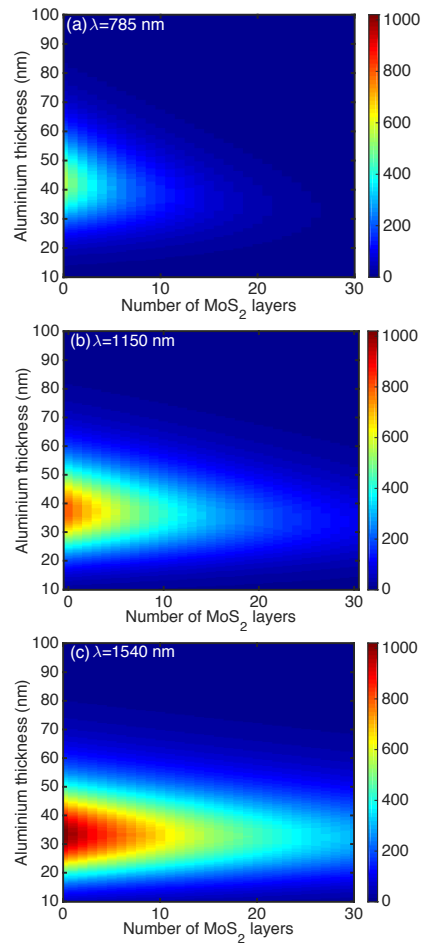


Fig. 5. Imaging sensitivity as a function of the number of MoS<sub>2</sub> layers and Al thickness at (a)  $\lambda = 785 \text{ nm}$ , (b)  $\lambda = 1150 \text{ nm}$  and (c)  $\lambda = 1540 \text{ nm}$ .

The sensing layer RI is another important parameter for the sensor performance. As shown in Fig. 6(a), the resonance angle increases with the sensing layer RI, which can be understood from



the SPR resonance condition [2]:

$$\frac{2\pi}{\lambda} n_p \sin \theta_{\text{SPR}} = \text{Re} \left\{ \frac{2\pi}{\lambda} \left( \frac{\epsilon_m n_s^2}{\epsilon_m + n_s^2} \right)^{1/2} \right\}, \quad (9)$$

where  $n_p$  is the RI of prism,  $\epsilon_m$  is the dielectric constant of metal film. The left-hand side of Eq. (9) is the propagation constant of the incident light, and the term on the right hand side is the real part of propagation constant of SPW. The propagation constant of the SPW increases with the RI of sensing layer, which leads to the increase in the resonance angle. In addition, the resonance angle also increases with the incident wavelength (Fig. 6(a)). For the sensor performance, the FWHM increases and the imaging sensitivity decreases with the sensing layer RI (see Fig. 6(b) and (c)).

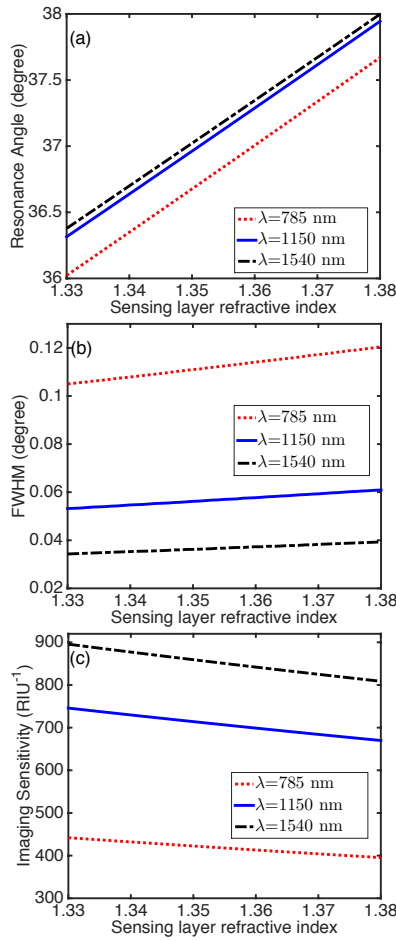


Fig. 6. (a) Resonance angle, (b) FWHM, and (c) imaging sensitivity as a function of the sensing layer refractive index at three different wavelengths,  $\lambda = 785$  nm, 1150nm and 1540 for monolayer MoS<sub>2</sub> based imaging sensor. The Al thickness is 38 nm.

Other 2D TMDC materials, like Molybdenum diselenide (MoSe<sub>2</sub>), Tungsten disulfide (WS<sub>2</sub>) and Tungsten diselenide (WSe<sub>2</sub>), have been proposed and demonstrated for sensing applications [23, 24, 37, 38]. It is interesting to compare the sensor performance of SPR imaging sensor with different TMDC materials. Here, we compare the imaging sensitivity and FWHM for SPR

imaging sensor with four TMDC materials ( $\text{MoS}_2$ ,  $\text{MoSe}_2$ ,  $\text{WS}_2$ , and  $\text{WSe}_2$ ) at three different wavelengths, as shown in Fig. 7 and 8, respectively. The thickness of Al film are taken from Fig. 3 that have been optimized for the three wavelengths: 42.8 nm for  $\lambda = 785$  nm, 37.6 nm for  $\lambda = 1150$  nm and 33.4 nm for  $\lambda = 1540$  nm. Similar to the  $\text{MoS}_2$ -based SPR imaging sensor, imaging sensitivity decreases while FWHM increases with the number of layers for  $\text{MoSe}_2$ -,  $\text{WS}_2$ -, and  $\text{WSe}_2$ -based imaging sensor. For  $\lambda = 785$  nm,  $\text{WSe}_2$  exhibits the highest imaging sensitivity with minimum FWHM, whereas  $\text{MoSe}_2$ -based sensor has the smallest sensitivity and maximum FWHM. At  $\lambda = 1150$  nm,  $\text{MoS}_2$  SPR imaging sensor has the maximum sensitivity as well as the minimum FWHM, same as the case of  $\lambda = 1540$  nm. For the other three TMDC materials at wavelengths  $\lambda = 1150$  nm and  $\lambda = 1540$  nm, they exhibit similar imaging sensitivity, and  $\text{WS}_2$ -based SPR imaging sensor has the maximum FWHM. Therefore, to obtain a high performance SPR imaging sensor, one can choose  $\text{WSe}_2$ -based sensor at  $\lambda = 785$  nm, while for wavelengths  $\lambda = 1150$  nm and  $\lambda = 1540$  nm,  $\text{MoS}_2$  is a better choice.

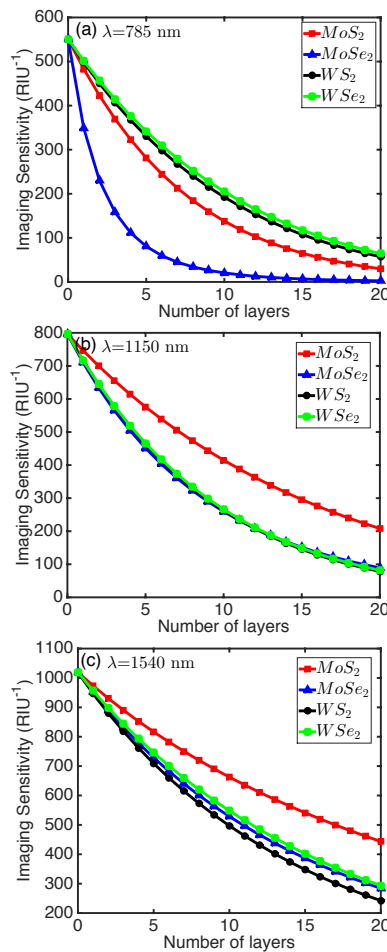


Fig. 7. Imaging sensitivity for SPR imaging sensor with multiple TMDC layers. (a)  $\lambda = 785$  nm with 42.8 nm thick Al film, (b)  $\lambda = 1150$  nm with 37.6 nm thick Al film, and (c)  $\lambda = 1540$  nm with 33.4 nm thick Al film.

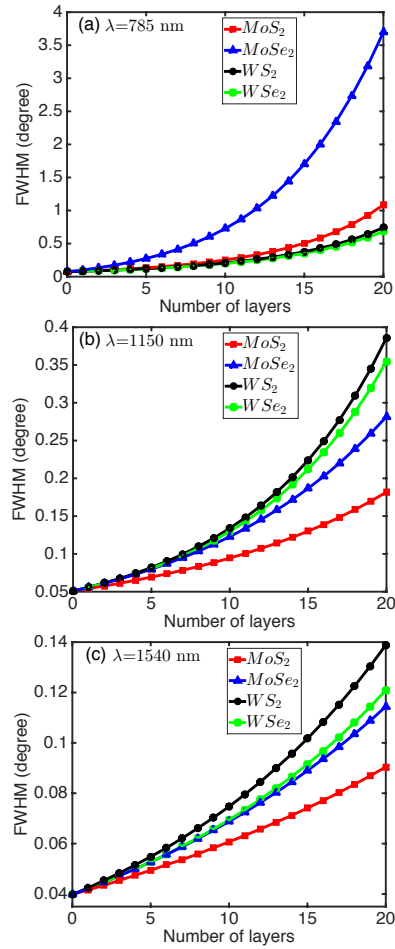


Fig. 8. FWHM for SPR imaging sensor with multiple TMDC layers. (a)  $\lambda = 785$  nm with 42.8 nm thick Al film, (b)  $\lambda = 1150$  nm with 37.6 nm thick Al film, and (c)  $\lambda = 1540$  nm with 33.4 nm thick Al film.

#### 4. Conclusion

In this work, an ultrahigh sensitive SPR imaging biosensor based on MoS<sub>2</sub>-on-Al is proposed. In the designed biosensor structure, MoS<sub>2</sub> layers are employed to inhibit the oxidation of Al thin film and as the recognition layer to capture biomolecules. Graphene-on-Al based sensor exhibits better sensor performance than that of the proposed sensor in the visible range, however, the MoS<sub>2</sub>-based SPR imaging biosensor overtakes its graphene counterparts in the near-infrared regime. It is found that the imaging sensitivity decreases with the number of MoS<sub>2</sub> layers applied, while the FWHM increases. A similar trend is observed with the RI of sensing layer. In addition, better sensor performance can be obtained at higher wavelength, where the imaging sensitivity can be as high as  $\sim 974 \text{ RIU}^{-1}$  at wavelength  $\lambda = 1540$  nm. Compared with other TMDC materials (MoSe<sub>2</sub>, WS<sub>2</sub>, and WSe<sub>2</sub>) based biosensor, biosensor based on WSe<sub>2</sub> shows the best sensor performance at wavelength  $\lambda = 785$  nm, while MoS<sub>2</sub>-based biosensor has better performance than the other three biosensors at wavelengths  $\lambda = 1150$  nm and  $\lambda = 1540$  nm. We believe that the present study will be helpful in designing a high performance SPR imaging sensor for chemical and biosensing applications.

**Funding**

Singapore ASTAR AME IRG (A1783c0011).